Hindawi Publishing Corporation
International Journal of Antennas and Propagation
Volume 2015, Article ID 345137, 11 pages
http://dx.doi.org/10.1155/2015/345137

Research Article

Designs and Performance Characteristics of Coated Nanotoroid Antennas

Sami Ur Rehman,[1] Junping Geng,[1] Richard W. Ziolkowski,[2] Ying Wang,[3] Xianling Liang,[1] and Ronghong Jin[1]

[1]*Department of Electronic Engineering, Shanghai Jiao Tong University, No. 800 Dongchuan Road, Shanghai 200240, China*
[2]*Electrical and Computer Engineering Department, University of Arizona, 1230 E. Speedway, Tucson, AZ 85721-0104, USA*
[3]*Ministry of Information of the Navy Command, No. 19 West Sanhuan Road, Beijing 100036, China*

Correspondence should be addressed to Junping Geng; gengjunp@sjtu.edu.cn

Received 16 February 2015; Accepted 27 May 2015

Academic Editor: Xianming Qing

The electromagnetic properties of a toroidal coated nanoparticle (T-CNP) antenna with an active core (doped with rare earth erbium Er^{3+} ions) are investigated. It is demonstrated that the active T-CNP acts as a strong dipole radiator at its resonance frequency when it is excited by a plane wave or an electric Hertzian dipole (EHD) radiating element. It is shown that in comparison to being a passive structure, the plane wave scattering cross section of the T-CNP can be increased by nearly 108 dBsm at its resonance frequency when it is active. Moreover, it is further demonstrated that the maximum peak of the power radiated by an EHD element in the presence of a properly designed active T-CNP is more than 120 dB over its value when radiating in free space; that is, its Purcell factor is 10^{12}.

1. Introduction

Because they behave as negative epsilon (ENG) media, metals at optical frequencies can exhibit a surface plasmonic character. Nanostructures which incorporate metals, including nanoparticles and arrays of them, have shown attractive properties [1–4] for applications in the areas of biology and medicine [1, 4–6], efficient solar cells [7–9], optical communications [10], high resolution microscopy [11, 12], and sensor [1, 13] technologies. By combining them with dielectric media doped, for instance, with the rare earth erbium ion, Er^{3+}, the resulting nanosized plasmonic particles can be designed to achieve highly subwavelength amplifiers and lasing elements [14–16].

Coated nanoparticles (CNP), which consist of spherical or cylindrical metallic nanoshells surrounding passive and active dielectric cores, as well as their complementary configurations, have been studied in almost all of their possible combinations. They can be designed to have novel optical properties that are geometrically tunable. If the core is filled with a lossless or lossy dielectric, the particle is called a passive CNP, the model of which has been discussed completely, for example, in [13]. When a passive CNP is excited by a plane wave, its performance can be naturally characterized by the maximum absorption (ACS), scattering (SCS), and extinction (ECS) cross sections, all of which depend on the radius of the core and the thickness of the metal film of the passive CNP. When the CNP is electrically small, the resulting radiated power distribution resembles that of a symmetrical dipole excited by the same electromagnetic wave. In addition to a variety of studies of exciting passive CNPs by plane waves, the electric Hertzian dipole (EHD) is another excitation choice that has also been studied extensively (e.g., [17]).

On the other hand, metals at optical frequencies show strong loss properties, which suppress, for instance, the SCS peak at the resonance frequency. To overcome the intrinsic losses associated with plasmonic structures, gain material has been incorporated into the dielectrics composing them. The resulting active CNPs have been studied extensively for their use as nanoamplifiers and nanolasers [14–16, 18–23]. The attractive features offered by active CNPs include not only radiated power enhancements, but also suppression effects

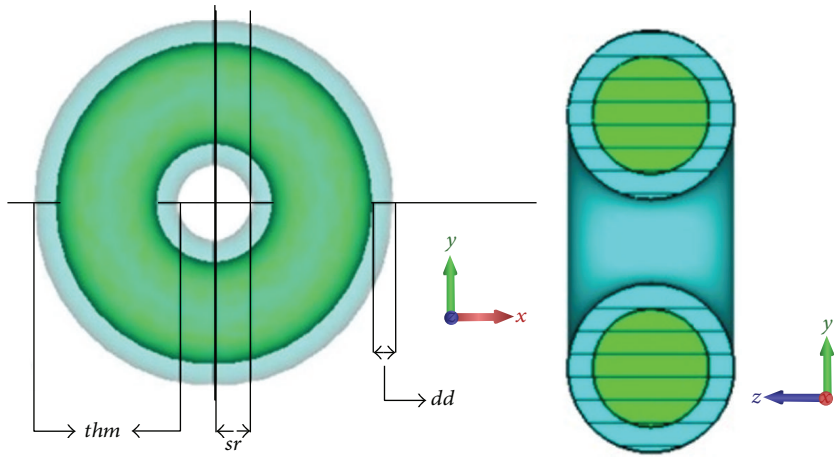

(a) Overhead view (b) Lateral view

Figure 1: Basic T-CNP model geometry.

[18, 23, 24]. Besides the CNP-based dipole radiators, a variety of other nanoantenna structures have been investigated over the past few years. These include optical dipoles [20, 25–31], monopoles [32, 33], bow-tie nanoantennas [31, 34–36], Yagi-Uda nanoantennas [37, 38], V-shaped nanoantennas [39], dimers as nanoantennas [40–44], dipole nanoantennas with matched loads [45, 46], and tunable nanoantennas [47–49].

The analyses of many of these basic nanoantenna structures have been based on the solutions of canonical problems and numerical simulations. Many of these structures remain far from practical realizations because of the lack of the necessary fabrication technologies. Nonetheless, these analyses provide much needed physical understanding. As nanofabrication techniques become more and more sophisticated, along with an increase in desired functionality, more complex coated structures (e.g., [50]) are now being considered. These more sophisticated nanostructures have far more complex material and structural characteristics. They can be modeled accurately with proven numerical simulators.

In this paper a novel toroidal structure, consisting of a gain impregnated silica core that is surrounded by a silver nanoshell coating, is studied. Both plane wave and electric Hertzian dipole (EHD) excitations are considered. It is shown that both the passive and active, electrically small toroidal coated nanoparticles (T-CNPs) can be designed to be resonant and that they radiate a basic dipole mode when they are resonant, yielding a strong linearly polarized field. Parameter studies of these designs are used to delineate the various properties of these optical nanoantennas, especially their enhancements of the total radiated power.

2. T-CNP Model

The basic T-CNP geometry is shown in Figure 1. The core is assumed to be silica (SiO_2) doped with rare earth erbium, Er^{3+}, ions. The nanoshell is assumed to be silver. The T-CNP is excited by both plane waves and the fields radiated by an EHD source.

2.1. Numerical Model. To simulate the T-CNP design shown in Figure 1, a commercial software package, CST Microwave Studio, was used. It is a computational electromagnetics simulation tool set which solves Maxwell's equations in the time domain based on the finite integration in time (FIT) technique, and in the frequency domain based on the finite element method (FEM) [51, 52]. Time domain methods are most suitable for wide band problems, while frequency domain methods are more appropriate for narrow band problems. Dispersive effects must be taken into account for any lossy, real, or artificial materials. The silver coating layer has properties that can be described by a thickness-dependent Drude model between 200 nm and 1800 nm [14]. In particular, the permittivity is decomposed into a size-dependent Drude response and an interband transition response. To incorporate this model into the CST solver, it was expressed in terms of a basic Drude permittivity in [21]. The gain model, which had to be implemented in CST's frequency domain solver, was described in detail in [19, 20]. The gain material is described in the frequency-domain CST solver by a modified Lorentz model of the permittivity [19, 20].

2.2. Plane Wave Excitation. For a plane wave excitation of the T-CNP, the behavior of the resulting scattered fields can be described by the scattering (SCS) and absorption (ACS) cross sections. The SCS is defined as the total integrated power contained in the scattered field normalized by their radiance of the incident field. The ACS is defined by the net flux through a surface surrounding the T-CNP normalized by the incident field irradiance [20]. Using Poynting's theorem and the total power scattered and absorbed by the structure, both the SCS and ACS can be expressed in terms of the ratio of the scattered and absorbed powers to the incident irradiance I_{inc} [20].

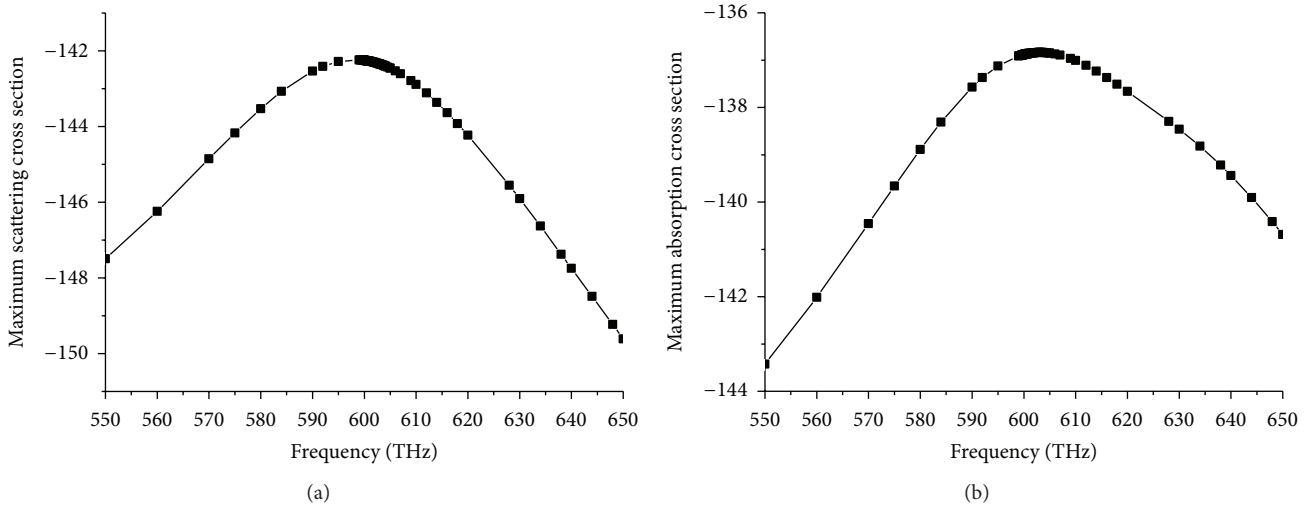

Figure 2: Excitation of the passive T-CNP by a plane wave polarized along the axis of the toroid. Maximum values of the (a) scattering (SCS) and (b) absorption (ACS) cross sections as a function of the excitation frequency.

2.3. EHD Excitation. Similarly, the response of the EHD-excited T-CNP system can be characterized by the total radiated power:

$$P_{\text{tot}} = \lim_{S\to\infty} \oiint_S \text{Re}\left\{\frac{1}{2}\vec{E}_{\text{tot}}(r,\theta,\varphi)\times\vec{H}^{*}_{\text{tot}}(r,\theta,\varphi)\right\}\cdot d\vec{S}, \quad (1)$$

where S is a closed surface that completely surrounds the EHD and the scatter. This quantity is readily calculated numerically using a cube surrounding the EHD and T-CNP system [21]. The total power radiated by an EHD of length d and current moment $p_s = I_0 d$ alone in free space has the well-known value [53]:

$$P_{\text{EHD}} = \frac{\eta_0\pi}{3}\left|\frac{p_s k_0}{2\pi}\right|^2 = \frac{\eta_0\pi}{3}\left|\frac{I_0 d}{\lambda}\right|^2, \quad (2)$$

where η_0 and k_0 are, respectively, the free space wave impedance and wave number. The behavior of the EHD/T-CNP nanoantenna system can then be described by the radiated power ratio, that is, the Purcell factor:

$$\text{PR} = \frac{P_{\text{tot}}}{P_{\text{EHD}}}. \quad (3)$$

3. Results for the Plane Wave Excitation

3.1. Passive T-CNP Excited by a z-Polarized Plane Wave. The silver coating layer in Figure 1 has a thickness denoted as *dd*. The inner radius of the torus is denoted as *sr*. The total thickness of the silver and the passive SiO_2 core medium is denoted as *thm*. The axis of the torus was taken to be along the z-axis. The T-CNP was excited by a vertically polarized plane wave; that is, the electric field vector is parallel to the z-axis and is propagating along the x-axis, as shown in Figure 1. The incident plane wave field is given as

$$\overrightarrow{E} = \hat{z}E_0\cos(\omega t - kx). \quad (4)$$

The electric field amplitude E_0 is assumed to be 1.0 V/m throughout this paper. On the basis of previous results and numerical models used to describe the behaviors of the passive and active spherical CNPs in [20] and the cylindrical-shaped CNPs (CC-CNPs) in [21], the thickness of the silver coating was set to *dd* = 6.0 nm. During the parameter sweeps, it was also observed that the peak location of the SCS in frequency changed as the parameters *sr* and *thm* were varied. The maximum SCS and ACS peaks were found to occur for *sr* = 11 nm and *thm* = 41 nm. The maximum SCS and ACS values for this optimized passive T-CNP as functions of the excitation frequency are shown in Figure 2. These results demonstrate that the resonance peak for the SCS is around 600 THz, as expected from prior studies. In particular, the peak value of the SCS is −142.24 dBsm at 599 THz.

The predicted results of the electric field, power density, current density and the electric and magnetic field energy densities for the passive T-CNP at its lowest order resonance frequency are shown in Figure 3. The total electric field distribution, as shown in Figure 3(a), is almost symmetric but is not quite because it also includes the incident field distribution. It demonstrates that the scattered field generated by the resonant T-CNP dominates the near-field behavior. The power flow distribution in Figure 3(b) shows how the resonant T-CNP has an SCS that is much larger than its geometrical size. It shows the electromagnetic power being channeled into the resonant T-CNP from all directions far away from its middle. The bulk currents are shown in Figure 3(c). They are flowing strongly in the silver shell of the resonant T-CNP with a pattern that radiates the fundamental electric dipole mode. The TM dipole mode of this T-CNP structure is oriented in the same direction as the polarization of the incident electric field. This feature also explains the electric field distribution in Figure 3(a). Similar effects are illustrated with the electric and magnetic field energy density distributions in Figures 3(d) and 3(e). The generation of the electric dipole mode at the resonance frequency is again

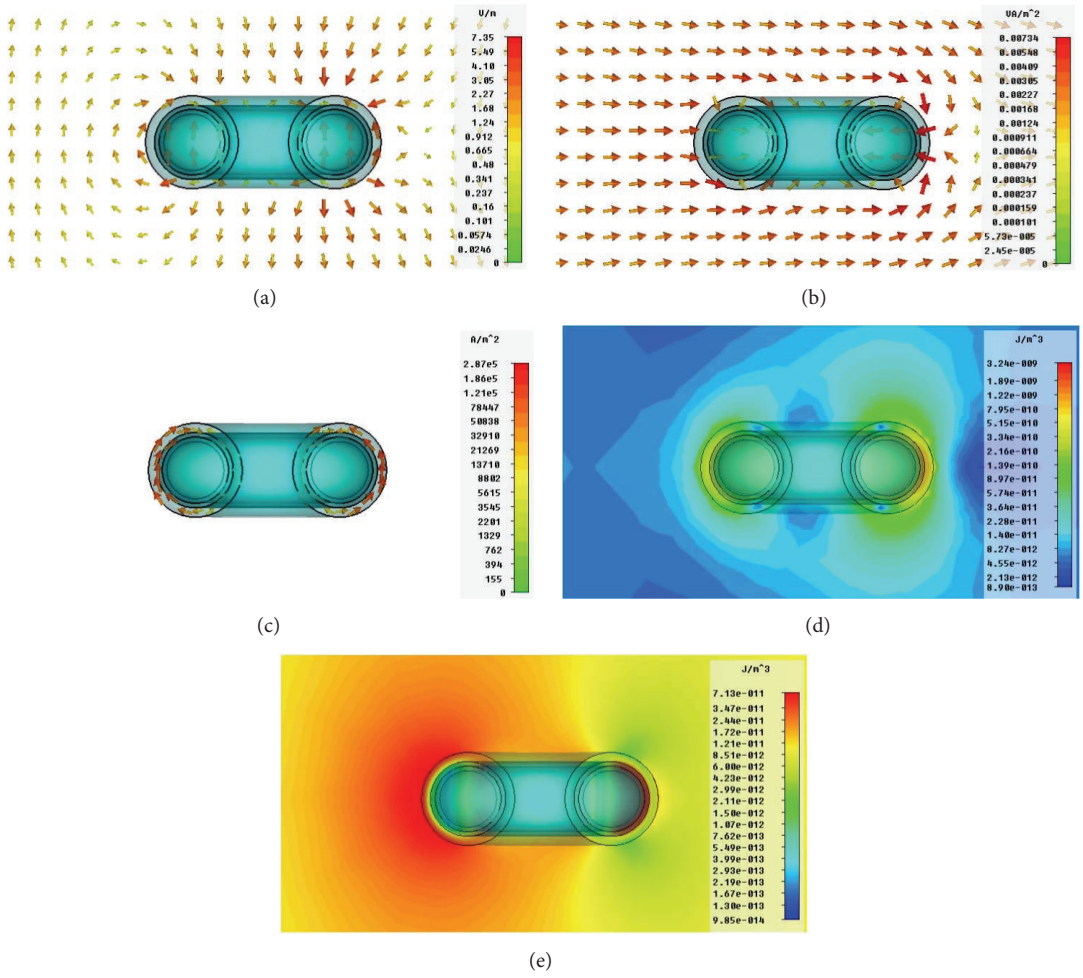

FIGURE 3: Simulated field distributions in the X-plane at $f = 599$ THz for the passive T-CNP with $sr = 11$ nm and $thm = 41$ nm. (a) Electric field, (b) power flow, (c) current density, (d) electric field energy density, and (e) magnetic field energy density.

confirmed with the three-dimensional (3D) SCS plot given in Figure 4.

3.2. Active T-CNP Excited by a z-Polarized Plane Wave. The configuration for the active T-CNP is geometrically the same as in the passive case and shown in Figure 1. The thickness of its silver metal shell is kept the same as that in the passive case; that is, $dd = 6$ nm. The excitation source is again the z-polarized plane wave given by (4). Thus, the T-CNP axis is again parallel to the electric field of the incident plane wave. The silver model is identical to the one used in the passive case; the gain model is identical to the one used previously in [19–22]. Following the same steps as those used in the passive case, the maximum response was achieved by optimizing the geometry and material parameters; that is, by sweeping the parameters sr and thm, the maximum response of the T-CNP was found. Those parameter sweeps (with $dd = 6.0$ nm) indicated that the maximum response is achieved with the values $sr = 11$ nm and $thm = 43$ nm. It was also assumed that the gain medium is depletion-free; that is, that all atoms in the gain region contribute to the scattering/radiation process. However in reality and because of depletion, the actual number of atoms contributing to the gain process may decrease in time. Consequently, our simulation results represent upper (lower) bounds on the scattering responses of the T-CNPs. Furthermore, only the coherent responses of the system are taken into consideration. Again, in a real experiment there may be a strong luminescence response arising from incoherent processes as the active medium is pumped. This background response can mask small coherent responses of interest [21]. Nevertheless, because our model takes into account the gain to produce the background response levels and our coherent response is several orders of magnitude above those levels, we expect that the predicted super resonance responses reported in this work would be readily observed in any active T-CNP scattering experiments.

The simulated maximum values of the SCS and ACS as functions of the excitation frequency for the optimized geometry are given in Figure 5. The SCS results shown in Figure 5 indicate that the resonance frequency occurs at 599.74 THz, where the peak SCS value is −108.11 dBsm. This result is significantly (~34.13 dBsm) higher than the peak

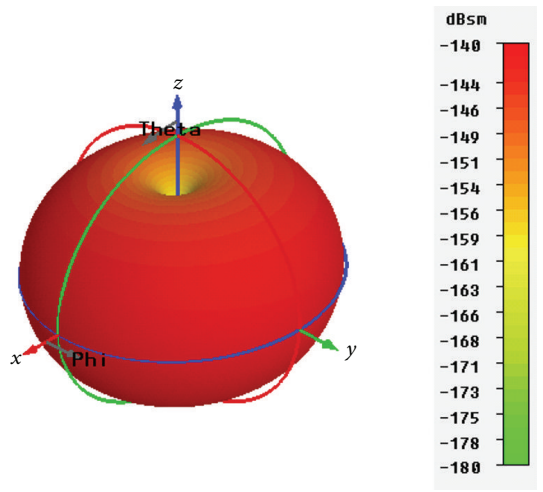

FIGURE 4: 3D plot of the far-field SCS behavior of passive T-CNP at the 599 THz resonance frequency.

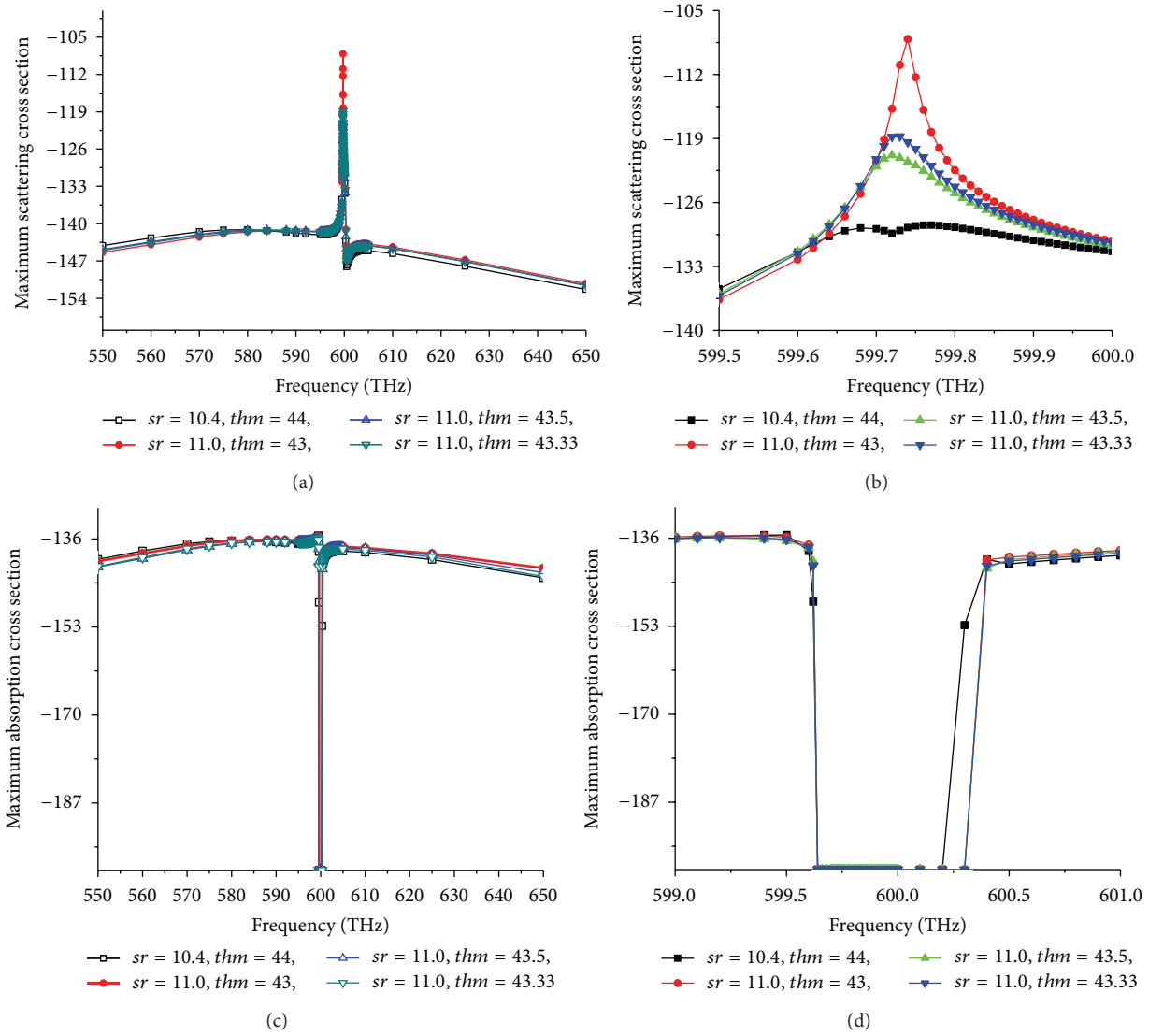

FIGURE 5: Simulated results for the optimized active T-CNP. (a) Maximum SCS values over a large frequency window, (b) zoom-in of (a) near the resonance frequency; and (c) maximum ACS values over a large frequency window, (d) zoom-in of (c) near the resonance frequency.

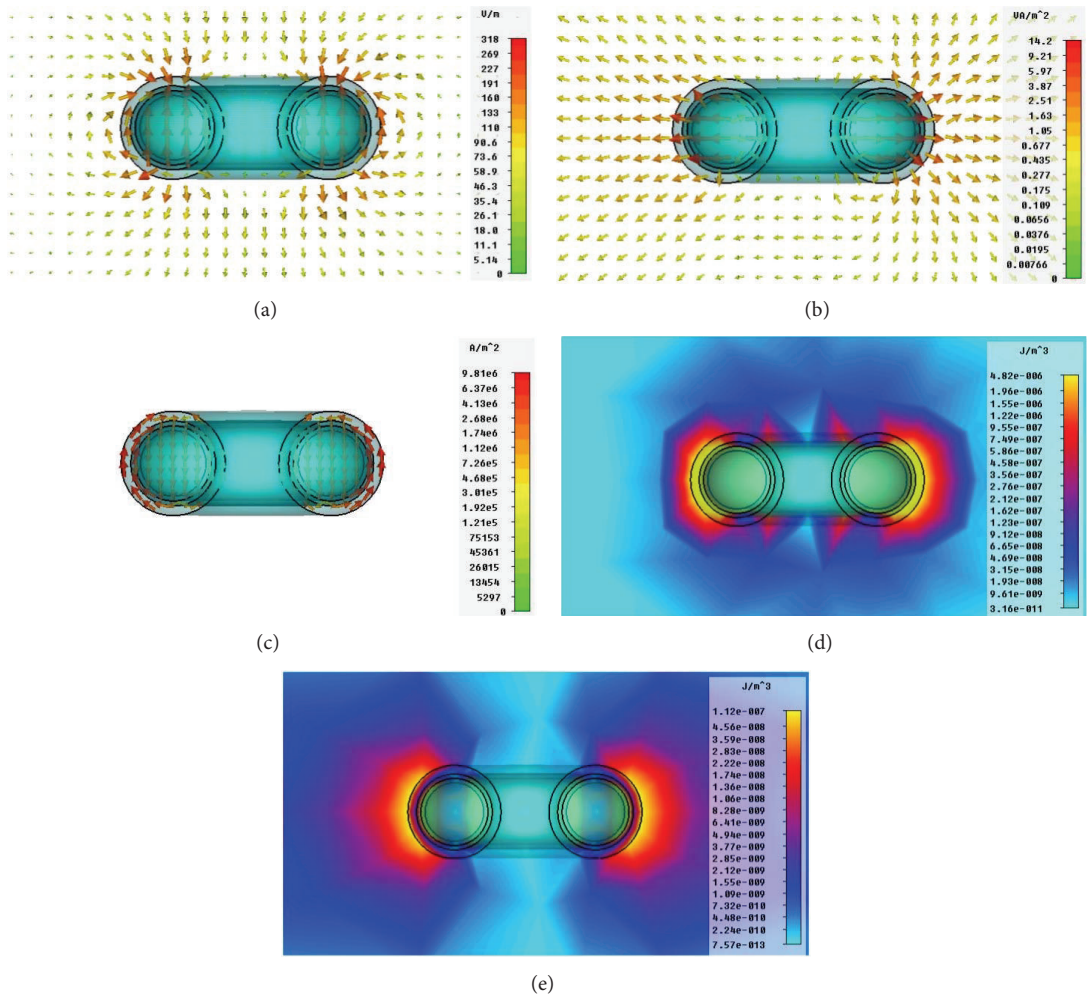

FIGURE 6: Simulated field distributions in the X-plane at $f = 599.74$ THz for the active T-CNP with $sr = 11$ nm and $thm = 43$ nm. (a) Electric field, (b) power flow, (c) current density, (d) electric field energy density, and (e) magnetic field energy density.

value for the passive case shown in Figure 2. Similarly the ACS values also decrease by a similar significant amount (63.16 dBsm) when compared with the passive case shown in Figure 2.

The simulated distributions of the electric field, power density, current density, and the electric and magnetic field energy densities at the resonant frequency, 599.74 THz, are shown in Figure 6. The electric field and power flow distributions in Figures 6(a) and 6(b), respectively, along with the far-field 3D SCS pattern given in Figure 7, clearly demonstrate that the active T-CNP is radiating in the electric dipole mode at its resonance frequency, but at much higher levels as compared to the passive case values. Figure 6(c) indicates that a large current density is generated in the core and a strong current loop is formed in the surrounding metal shell at resonance. The resonant current in the core is a combination of the conduction and displacement currents. The conduction current occurs in the core of the active T-CNP because of the conductivity (associated with the loss term) introduced by the gain model. This behavior in the active T-CNP is

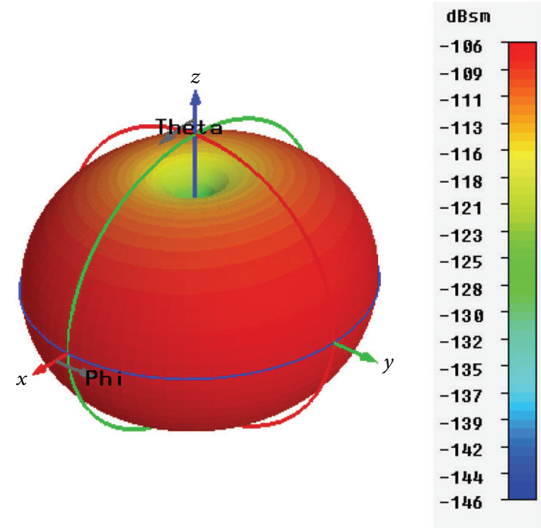

FIGURE 7: 3D plot of the far-field SCS behavior of the active T-CNP at its resonance frequency, 599.74 THz.

a significant contrast to the much weaker currents that only flow in the metallic shell at nonresonant frequencies and in all of the passive cases. As a consequence, the strong currents dominate the radiation process; and, as shown in Figure 6(b), the power is clearly flowing away from the center of T-CNP. The electric and magnetic field energy distributions shown, respectively, in Figures 6(d) and 6(e) also confirm the electric dipole nature of the behavior of active T-CNP at its resonance frequency.

Note that when the amplification becomes significantly large, as it does at the resonance frequency, the electric fields in the core region are extremely large. The T-CNP as an electrically small resonator, like its spherical and cylindrical counterparts, is facilitated and formed by the juxtaposition of the ENG and regular double positive (DPS) materials. The metallic coated core is purposely chosen to emphasize this resonator effect. The complementary structure has a much weaker field confinement and thus requires more gain to achieve amplification [54]. Because of these large fields and the presence of the effective conductivity introduced by the loss component of the gain model, the conduction currents are large in the core as noted previously. Furthermore, because of the difference in signs of the permittivity in the core and in the shell, the current densities in both regions are of opposite direction as illustrated in Figure 6(c).

3.3. T-CNP Excited by an EHD. After establishing the resonance frequency and the fundamental dipole radiation process of the passive and active T-CNP under plane wave excitation, the behavior of the active structure was examined using an EHD as the source of excitation. The impact on the T-CNP nanoamplifier performance arising from differences in the location of the EHD was of particular interest. It was expected that the outcomes of these studies would accentuate how well the T-CNP would act as a nanoamplifier in a nanosensor application. For instance, a fluorescing atom or molecule would act as a dipole in its transition from an excited to a lower energy state [20, 21]. By tuning the resonance of the T-CNP to the corresponding transition frequency, one would then achieve a significant amplification of the fluorescent response of that atom or molecule. On the other hand, if the atom or molecule would fall into the center of the toroid or just outside of it, the T-CNP would still produce a significantly amplified emission signal? If the amplification level was essentially independent of the location of the effective EHD, the T-CNP would make an ideal nanoamplifier for the resulting nanosensor system.

The dimensions and material properties of the active T-CNP were kept exactly the same for the EHD excitation as those utilized in the optimized plane wave excitation case, that is, $sr = 11$ nm, $thm = 43$ nm, and $dd = 6.0$ nm. It was expected that the resonance frequency associated with the EHD excitation would be the same or only slightly different from its plane wave excitation value. The fluorescing emitter was assumed to be an EHD oriented along the axis of the toroid to achieve its maximum response. It was realized numerically as a small z-directed current element (oriented parallel to the axis of the toroid) located at all of the locations

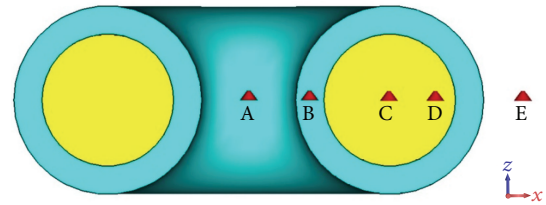

Figure 8: The EHD locations along the horizontal center line of the toroidal structure which were scanned to determine the impact of the source location on the active T-CNP performance characteristics. As illustrated, the EHD is oriented along the axis of the toroid.

shown in Figure 8. The current dipole moment of the EHD was held fixed in all cases to $I_0 d = 2 \times 10^{-12}$ A-m. Not only were the center-of-the-toroid and just outside-the-toroid locations considered, but also locations in the shell and within the core. Again, these were selected as comparison cases to establish how well the active T-CNP would act as a nanoamplifier.

The response of the active T-CNP excited by the EHD was characterized by the total power radiated by the system using a cube surrounding the overall (EHD and T-CNP) system [21]. The power radiated by the EHD alone was obtained in the same manner. The calculated radiated power ratios (3) for the EHD location points A, B, C, D, and E indicated in Figure 8 as functions of the excitation frequency are shown in Figure 9. The EHD locations starting from the geometric center of the T-CNP were precisely $x = 0$ (A), $x = 14$ nm (B), $x = 32.5$ nm (C), $x = 43.5$ nm (D), and $x = 57$ nm (E). It is clear from these radiated power ratio results that there is a large resonance peak close to 600 THz. In fact, all of the resonances occur at 599.74 THz, the same frequency as found for the plane wave excitation case. The maximum value of the radiated power ratio is 128.47 dB when the T-CNP is excited by the EHD at point D, inside the core but offset from the core center and closer to the inside wall of the silver shell. This off-center result is very similar to the EHD results obtained for the active cylindrical CNP [21]. The peak value at point A is 113.14 dB; at point E is 112.21 dB. While these peak values are not as large as the one obtained when the EHD was located in the core, they are nonetheless very large and emphasize the usefulness of the active T-CNP as a nanoamplifier. As one would expect, the peak values decrease as the EHD location moves further away for the T-CNP where the coupling of the EHD to it would be much less.

The field distributions and vector fields, when the EHD is located at the offset point D and excites the active T-CNP at its resonance frequency, 599.74 THz, are shown in Figure 10. Again, the electric field, power density, current density, and the electric and magnetic field energy densities are displayed. Note that they are all symmetric and have the anticipated dipole mode form. The local electric field in Figure 10(a) has the expected dipolar form. The power is radiating strongly outward away from the active T-CNP in Figure 10(b). Bulk currents at the resonance frequency are again clearly flowing in the gain material in Figure 10(c), as well as in the opposite

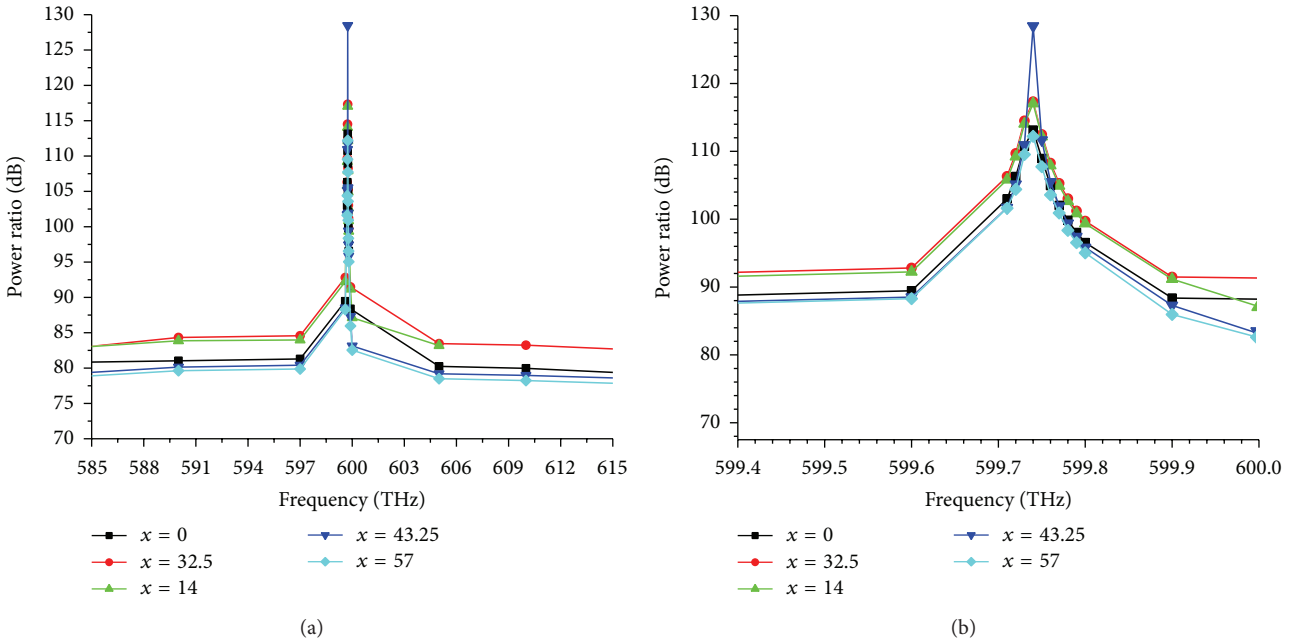

FIGURE 9: Results for radiated power ratio (Purcell factor) for the active T-CNP as a function of the frequency for the different EHD locations shown in Figure 8. (a) Large frequency window and (b) zoom-in near the resonance frequency.

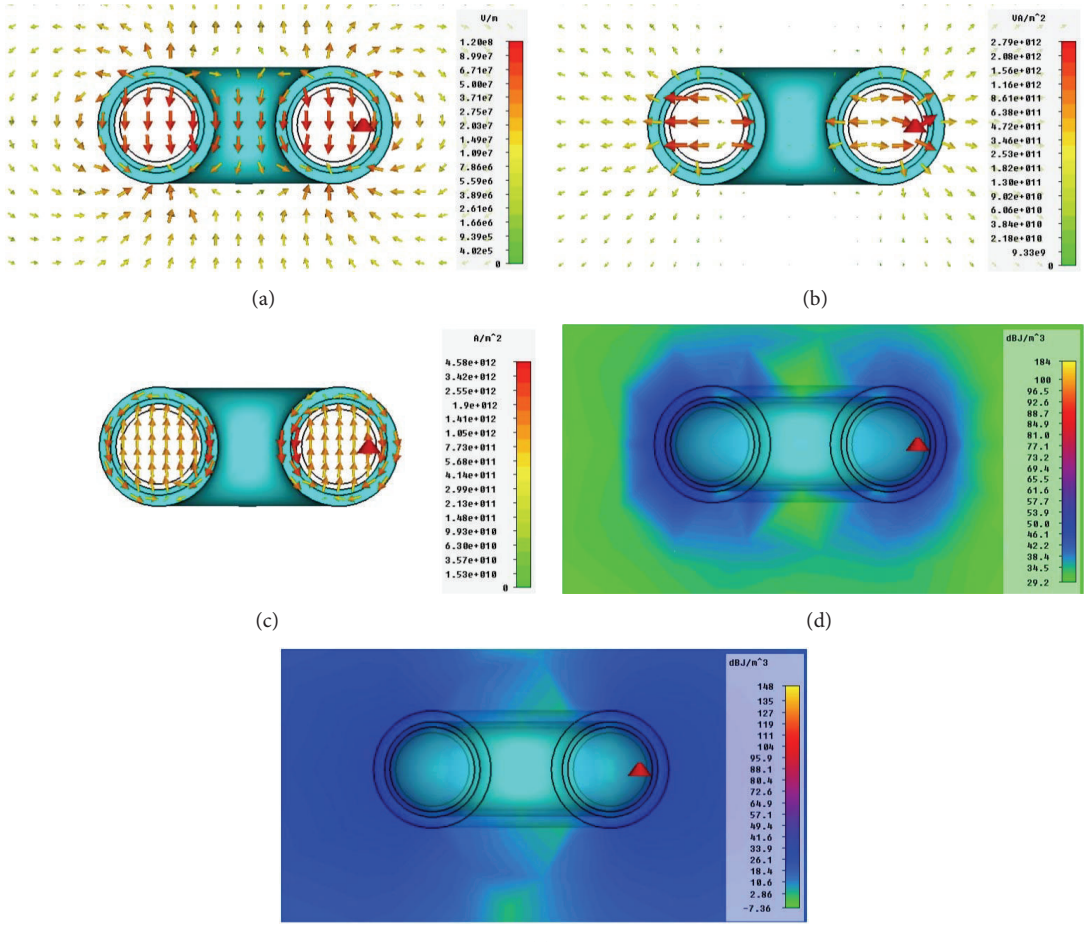

FIGURE 10: Simulated field distributions in the X-plane at $f = 599.74$ THz for the active T-CNP excited with the EHD at position D with $sr = 11$ nm and $thm = 43$ nm. (a) Electric field, (b) power flow, (c) current density, (d) electric field energy density, and (e) magnetic field energy density.

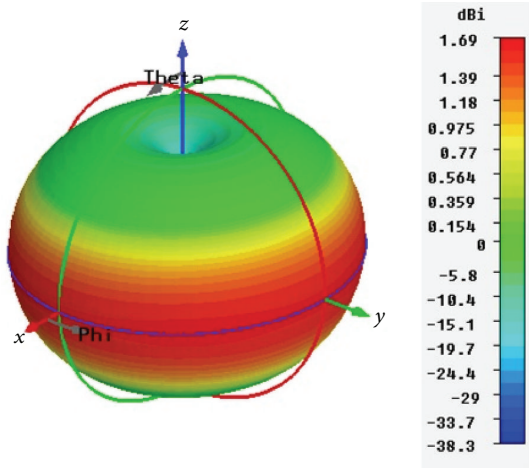

Figure 11: 3D plot of the far-field behavior at $f = 599.74$ THz, of T-CNP excited by an EHD at point D.

direction in the silver shell. The field energy densities are concentrated in and around the gain-impregnated core. As shown in Figure 11, the 3D directivity pattern is clearly a result of the electric dipole mode dominance of the radiation process. The same behaviors are realized for all of the locations, A–E, of the EHD.

4. Conclusions

An investigation of the electromagnetic behavior of passive and active, toroid shaped, and coated nanoparticles was presented. Using an experimentally validated frequency domain simulator, results for the plane wave excitation of both passive and active T-CNPs were considered. It was shown that the active T-CNP dramatically enhances the SCS and ACS values at its resonance frequency. An EHD excitation of the active T-CNP was also considered and studied by varying the locations of the EHD. It was demonstrated that whether the active T-CNPs were excited by plane wave or EHD fields, they could be designed to be resonant and their radiated field response was that of the fundamental electric dipole mode. The scattering cross section for the optimized T-CNP excited by a plane wave was increased by 108 dBsm at resonance from the background. The maximum of the total radiated power ratio (Purcell factor) for the corresponding EHD excitation was increased by 120 dB. These results confirm the potential usefulness of active T-CNPs for nanosensor applications.

Conflict of Interests

The authors declare that there is no conflict of interests regarding the publication of this paper.

Acknowledgments

This work was supported by the National Natural Science Foundation (61201058, 61471240), the Research and Innovation Project of Shanghai Education Commission (12Z1120 30001), and the Scientific Research Foundation for Returned Overseas Chinese Scholars, the State Quality Inspection Administration of Science and Technology Project under Grant 2013QK127, State Education Ministry, and the Project of "SMC Excel lent Young Faculty".

References

[1] P. K. Jain, X. Huang, I. H. El-Sayed, and M. A. El-Sayed, "Noble metals on the nanoscale: optical and photo thermal properties and some applications in imaging, sensing, biology, and medicine," *Accounts of Chemical Research*, vol. 41, no. 12, pp. 1578–1586, 2008.

[2] J. A. Gordon and R. W. Ziolkowski, "CNP optical metamaterials," *Optics Express*, vol. 16, no. 9, pp. 6692–6716, 2008.

[3] B. García-Cámara, F. Moreno, F. González, and O. J. F. Martin, "Light scattering by an array of electric and magnetic nanoparticles," *Optics Express*, vol. 18, no. 10, pp. 10001–10015, 2010.

[4] N. J. Halas, "Plasmonics: an emerging field fostered by nano letters," *Nano Letters*, vol. 10, no. 10, pp. 3816–3822, 2010.

[5] A. W. H. Lin, N. A. Lewinski, J. L. West, N. J. Halas, and R. A. Drezek, "Optically tunable nanoparticle contrast agents for early cancer detection: model-based analysis of gold nanoshells," *Journal of Biomedical Optics*, vol. 10, no. 6, Article ID 064035, 2005.

[6] X. Liu and Q. Huo, "A washing-free and amplification-free one-step homogeneous assay for protein detection using gold nanoparticle probes and dynamic light scattering," *Journal of Immunological Methods*, vol. 349, no. 1-2, pp. 38–44, 2009.

[7] K. R. Catchpole and A. Polman, "Plasmonic solar cells," *Optics Express*, vol. 16, no. 26, pp. 21793–21800, 2008.

[8] R. A. Pala, J. White, E. Barnard, J. Liu, and M. L. Brongersma, "Design of plasmonic thin-film solar cells with broadband absorption enhancements," *Advanced Materials*, vol. 21, no. 34, pp. 3504–3509, 2009.

[9] H. A. Atwater and A. Polman, "Plasmonics for improved photovoltaic devices," *Nature Materials*, vol. 9, no. 3, pp. 205–213, 2010.

[10] G. Shvets, S. Trendafilov, J. B. Pendry, and A. Sarychev, "Guiding, focusing, and sensing on the subwavelength scale using metallic wire arrays," *Physical Review Letters*, vol. 99, no. 5, Article ID 053903, 4 pages, 2007.

[11] A. Grbic, L. Jiang, and R. Merlin, "Near-field plates: subdiffraction focusing with patterned surfaces," *Science*, vol. 320, no. 5875, pp. 511–513, 2008.

[12] S. Kawata, Y. Inouye, and P. Verma, "Plasmonics for near-field nano-imaging and superlensing," *Nature Photonics*, vol. 3, no. 7, pp. 388–394, 2009.

[13] J. A. Gordon and R. W. Ziolkowski, "Investigating functionalized active coated nano-particles for use in nano-sensing applications," *Optics Express*, vol. 15, no. 20, pp. 12562–12582, 2007.

[14] J. A. Gordon and R. W. Ziolkowski, "The design and simulated performance of a coated nano-particle laser," *Optics Express*, vol. 15, no. 5, pp. 2622–2653, 2007.

[15] M. I. Stockman, "The spaser as a nanoscale quantum generator and ultrafast amplifier," *Journal of Optics A: Pure and Applied Optics*, vol. 12, no. 2, Article ID 024004, 2010.

[16] I. Liberal, I. Ederra, R. Gonzalo, and R. W. Ziolkowski, "Induction theorem analysis of resonant nanoparticles: design of a Huygens source nanoparticle laser," *Physical Review Applied*, vol. 1, no. 4, Article ID 044002, 2014.

[17] S. Arslanagić, R. W. Ziolkowski, and O. Breinbjerg, "Radiation properties of an electric Hertzian dipole located near-by concentric metamaterial spheres," *Radio Science*, vol. 42, Article ID RS6S16, 2007.

[18] S. Arslanagić and R. W. Ziolkowski, "Active coated nano-particle excited by an arbitrarily located electric Hertzian dipole-resonance and transparency effects," *Journal of Optics A: Pure and Applied Optics*, vol. 12, no. 2, Article ID 024014, 2010.

[19] J. Geng, R. W. Ziolkowski, S. Cambell, R. Jin, and X. Liang, "Studies of nanometer antennas incorporating gain material using CST," in *Proceedings of the IEEE International Symposium on Antennas and Propagation and USNC/URSI National Radio Science Meeting (APSURSI '11)*, pp. 1624–1627, Spokane, Wash, USA, July 2011.

[20] J. Geng, R. W. Ziolkowski, R. Jin, and X. Liang, "Numerical study of the near-field and far-field properties of active open cylindrical coated nanoparticle antennas," *IEEE Photonics Journal*, vol. 3, no. 6, pp. 1093–1110, 2011.

[21] J. Geng, R. W. Ziolkowski, R. Jin, and X. Liang, "Detailed performance characteristics of vertically polarized, cylindrical, active coated nano-particle antennas," *Radio Science*, vol. 47, Article ID RS2013, 2012.

[22] J. Geng, D. Chen, R. Jin, X. Liang, J. Tang, and R. W. Ziolkowski, "Study of active coated nano-toroid antennas," in *Proceedings of the International Workshop on Antenna Technology (iWAT '13)*, pp. 154–157, Karlsruhe, Germany, March 2013.

[23] S. Arslanagić and R. W. Ziolkowski, "Influence of active nano particle size and material composition on multiple quantum emitter enhancements: their enhancement and jamming effects," *Progress in Electromagnetics Research*, vol. 149, pp. 85–99, 2014.

[24] S. Arslanagić and R. W. Ziolkowski, "Jamming of quantum emitters by active coated nan-oparticles," *IEEE Journal on Selected Topics in Quantum Electronics*, vol. 19, no. 3, Article ID 4800506, 2013.

[25] J. N. Farahani, D. W. Pohl, H.-J. Eisler, and B. Hecht, "Single quantum dot coupled to a scanning optical antenna: a tunable superemitter," *Physical Review Letters*, vol. 95, no. 1, Article ID 017402, 2005.

[26] E. Cubukcu, E. A. Kort, K. B. Crozier, and F. Capasso, "Plasmonic laser antenna," *Applied Physics Letters*, vol. 89, no. 9, Article ID 093120, 2006.

[27] S. Kuhn, U. Hkanson, L. Rogobete, and V. Sandoghdar, "Enhancement of single-molecule fluorescence using a gold nanoparticle as an optical nano antenna," *Physical Review Letters*, vol. 97, no. 1, Article ID 017402, 2006.

[28] L. Novotny, "Effective wavelength scaling for optical antennas," *Physical Review Letters*, vol. 98, no. 26, Article ID 266802, 2007.

[29] J. Aizpurua, G. W. Bryant, L. J. Richter, F. J. García de Abajo, B. K. Kelley, and T. Mallouk, "Optical properties of coupled metallic nanorods for field-enhanced spectroscopy," *Physical Review B*, vol. 71, no. 23, Article ID 235420, pp. 235–420, 2005.

[30] P. Mühlschlegel, H.-J. Eisler, O. J. F. Martin, B. Hecht, and D. W. Pohl, "Resonant optical antennas," *Science*, vol. 308, no. 5728, pp. 1607–1609, 2005.

[31] H. Fischer and O. J. F. Martin, "Engineering the optical response of plasmonic nanoantennas," *Optics Express*, vol. 16, no. 12, pp. 9144–9154, 2008.

[32] T. H. Taminiau, R. J. Moerland, F. B. Segerink, L. Kuipers, and N. F. van Hulst, "$\lambda/4$ Resonance of an optical monopole antenna probed by single molecule fluorescence," *Nano Letters*, vol. 7, no. 1, pp. 28–33, 2007.

[33] T. H. Taminiau, F. B. Segerink, and N. F. van Hulst, "A monopole antenna at optical frequencies: single-molecule near-field measurements," *IEEE Transactions on Antennas and Propagation*, vol. 55, no. 11, pp. 3010–3017, 2007.

[34] D. P. Fromm, A. Sundaramurthy, P. James Schuck, G. Kino, and W. E. Moerner, "Gap-dependent optical coupling of single 'bowtie' nanoantennas resonant in the visible," *Nano Letters*, vol. 4, no. 5, pp. 957–961, 2004.

[35] L. Wang, S. M. Uppuluri, E. X. Jin, and X. Xu, "Nanolithography using high transmission nanoscale bowtie apertures," *Nano Letters*, vol. 6, no. 3, pp. 361–364, 2006.

[36] A. Sundaramurthy, P. J. Schuck, N. R. Conley, D. P. Fromm, G. S. Kino, and W. E. Moerner, "Toward nanometer-scale optical photolithography: utilizing the near-field of bowtie optical nanoantennas," *Nano Letters*, vol. 6, no. 3, pp. 355–360, 2006.

[37] J. Li, A. Salandrino, and N. Engheta, "Shaping light beams in the nanometer scale: a Yagi-Uda nano antenna in the optical domain," *Physical Review B*, vol. 76, no. 24, Article ID 245403, 2007.

[38] T. H. Taminiau, F. D. Stefani, and N. F. Van Hulst, "Enhanced directional excitation and emission of single emitters by a nano-optical Yagi-Uda antenna," *Optics Express*, vol. 16, no. 14, pp. 10858–10866, 2008.

[39] J. Yang, J. Zhang, X. Wu, and Q. Gong, "Electric field enhancing properties of the V-shaped optical resonant antennas," *Optics Express*, vol. 15, no. 25, pp. 16852–16859, 2007.

[40] L. Rogobete, F. Kaminski, M. Agio, and V. Sandoghdar, "Design of plasmonic nanoantennae for enhancing spontaneous emission," *Optics Letters*, vol. 32, no. 12, pp. 1623–1625, 2007.

[41] O. L. Muskens, V. Giannini, J. A. Sánchez-Gil, and J. G. Rivas, "Strong enhancement of the radiative decay rate of emitters by single plasmonic nanoantennas," *Nano Letters*, vol. 7, no. 9, pp. 2871–2875, 2007.

[42] R. M. Bakker, A. Boltasseva, Z. Liu et al., "Near-field excitation of nanoantenna resonance," *Optics Express*, vol. 15, no. 21, pp. 13682–13688, 2007.

[43] O. L. Muskens, V. Giannini, J. A. Sánchez-Gil, and J. Gómez Rivas, "Optical scattering resonances of single and coupled dimer plasmonic nanoantennas," *Optics Express*, vol. 15, no. 26, pp. 17736–17746, 2007.

[44] A. Alú and N. Engheta, "Hertzian plasmonic nanodimer as an efficient optical nanoantenna," *Physical Review B—Condensed Matter and Materials Physics*, vol. 78, no. 19, Article ID 195111, 2008.

[45] A. Alú and N. Engheta, "Tuning the scattering response of optical nanoantennas with nanocircuit loads," *Nature Photonics*, vol. 2, no. 5, pp. 307–310, 2008.

[46] M. L. Brongersma, "Plasmonics: engineering optical nanoantennas," *Nature Photonics*, vol. 2, no. 5, pp. 270–272, 2008.

[47] G. Lévêque and O. J. F. Martin, "Tunable composite nanoparticle for plasmonics," *Optics Letters*, vol. 31, no. 18, pp. 2750–2752, 2006.

[48] K. H. Su, Q. H. Wei, and X. Zhang, "Tunable and augmented plasmon resonances of Au/SiO_2/Au nanodisks," *Applied Physics Letters*, vol. 88, no. 6, Article ID 063118, 2006.

[49] J. Merlein, M. Kahl, A. Zuschlag et al., "Nanomechanical control of an optical antenna," *Nature Photonics*, vol. 2, no. 4, pp. 230–233, 2008.

[50] B. Khlebtsov, E. Panfilova, V. Khanadeev et al., "Nanocomposites containing silica-coated gold-silver nanocages and Yb-2,4-dimethoxyhematoporphyrin: multifunctional capability of

IR-luminescence detection, photosensitization, and photothermolysis," *ACS Nano*, vol. 5, no. 9, pp. 7077–7089, 2011.

[51] https://www.cst.com/Products/CSTMWS/Solvers.

[52] T. Weiland, "Time domain electromagnetic field computation with finite difference methods," *International Journal of Numerical Modelling: Electronic Networks, Devices and Fields*, vol. 9, no. 4, pp. 295–319, 1996.

[53] C. A. Balanis, *Antenna Theory: Analysis and Design*, John Wiley & Sons, New York, NY, USA, 3rd edition, 2005.

[54] S. D. Campbell and R. W. Ziolkowski, "Impact of strong localization of the incident power density on the nano-amplifier characteristics of active coated nano-particles," *Optics Communications*, vol. 285, no. 16, pp. 3341–3352, 2012.